A generally applicable hybrid unsteady Reynolds-averaged Navier–Stokes closure scaled by turbulent structures

Physics of Fluids

A generally applicable hybrid unsteady Reynolds-averaged Navier–Stokes closure scaled by turbulent structures

Cite as: Phys. Fluids **33**, 105117 (2021); https://doi.org/10.1063/5.0065203
Submitted: 30 July 2021 • Accepted: 13 September 2021 • Published Online: 14 October 2021

Giancarlo Lenci, Jinyong Feng and Emilio Baglietto

Physics of Fluids ARTICLE scitation.org/journal/phf

A generally applicable hybrid unsteady Reynolds-averaged Navier–Stokes closure scaled by turbulent structures

Cite as: Phys. Fluids **33**, 105117 (2021); doi: 10.1063/5.0065203
Submitted: 30 July 2021 · Accepted: 13 September 2021 ·
Published Online: 14 October 2021

Giancarlo Lenci,[1,2,a)] Jinyong Feng,[1] and Emilio Baglietto[1]

AFFILIATIONS

[1]Department of Nuclear Science and Engineering, Massachusetts Institute of Technology, 77 Massachusetts Ave., Cambridge, Massachusetts 02139, USA
[2]Dominion Engineering, Inc., 12100 Sunrise Valley Dr., Suite 220, Reston, Virginia 20191, USA

[a)]**Author to whom correspondence should be addressed:** glenci@domeng.com

ABSTRACT

This work demonstrates a strategy for hybrid turbulence modeling that relies on parameters identifying flow structures to regulate the model's level of scale resolution, independent of the computational grid and user input. The approach can be classified as second-generation unsteady Reynolds-averaged Navier–Stokes (URANS), where it is assumed that increased scale resolution inside rapidly deformed turbulence regions can consistently reduce modeling error compared to basic URANS closures. The methodology selects flow structures by evaluating the second invariant of the velocity gradient tensor in the resolved field. The functions used for this purpose are similar to techniques applied in topology studies to identify coherent structures. The proposed formulation extends a baseline nonlinear eddy-viscosity URANS model and achieves completeness by means of a differential Lagrangian operator that approximates a locally computed average. The model addresses the lack of general applicability deriving from globally filtering at small scales by reverting to the baseline URANS in flow locations with low acceleration, in which the URANS solution achieves best accuracy. Three flow test cases are presented, demonstrating substantial accuracy enhancement over the baseline URANS on the same grid sizes. Results obtained with this new closure demonstrate robust applicability to internal flows, showing large-eddy simulation (LES)-like statistics on coarse RANS computational grids. The observed increase in computational cost compared to the baseline URANS is only 3% to 24%, which represents almost two orders of magnitude reduction from LES.

I. INTRODUCTION

The effectiveness of computational fluid dynamics (CFD) simulations of complex turbulent flows is still limited by the trade-off between accuracy and computational cost. As a consequence, many industrial CFD simulations at a high Reynolds number must resort to low-cost Reynolds averaged Navier–Stokes (RANS) models or their unsteady version (URANS). RANS/URANS closures in the form of two-equation models are easy to use and widely adopted, even outside validated domains, including in optimization and predictive analysis. However, in such flow problems, the condition of turbulent equilibrium required by these basic RANS/URANS solvers is often not satisfied locally; phenomena such as strong pressure gradients, flow separation, jets, and swirls often impair the accuracy of the method. Two-equation URANS models are valued for their robustness, expressed as a low sensitivity of results to small changes in the simulation conditions and grid resolution. These features derive from the averaged nature of the constituent equations and their diffusive character and justify the wide use of URANS models despite their well-recognized shortcomings in accuracy and flow description.

While direct numerical simulation (DNS) remains a tool for turbulence research,[1] large-eddy simulation (LES) can address many of the discussed flow challenges at the expense of high computational cost—often not attainable for industrial applications. LES uses filtered equations to resolve turbulent eddies down to the discretization limits, leaving the effects of smaller fluctuations to be modeled by subgrid-scale (SGS) closures.[2–4] The assumption of nearly homogeneous SGS turbulence establishes the requirement for LES filtering to happen in the low inertial subrange, enforcing very tight discretization constraints. Hardware limitations, together with the need to support iterative design and optimization jointly with uncertainty quantification,

prevent LES from becoming the standard simulation tool for complex turbulent flows in large industrial simulation domains.[5] Hybrid concepts have been proposed since the mid-1990s to bridge this simulation gap, starting with very-large-eddy simulation (VLES) by Speziale[6] and detached-eddy simulation (DES) by Spalart *et al.*[7] The two models modify the baseline URANS closure by activating scale-resolving features as a function of either grid size or wall distance. In both cases, the LES equations are not used directly, rather the models aim at reaching an LES-like behavior in hybrid activation zones. In the last two decades, many further hybrid models have been proposed, but despite notable examples of successful applications,[8–10] no hybrid turbulence concept yet provides a generic, reliable alternative to URANS or LES closures in industrial simulations.

While a large number of variants exist, they can be generally classified, following Fröhlich and von Terzi,[8] into segregated, interfaced and blended methods. In segregated models, URANS and LES equations are employed in specific sub-domains of the flow field that are manually fixed before the computation. The solution's accuracy is highly sensitive to the treatment of the discontinuity between the LES and URANS fields at the interface.[11] In interface-type models, a smooth transition is obtained between URANS and LES, adopting an interface function based on characteristic length- or time-scales, or more straightforwardly distance from the wall. The hybrid turbulent stress tensor can be expressed as follows:

$$\tau_{ij} = f_I \tau_{ij}^{\mathrm{URANS}} + (1 - f_I)\tau_{ij}^{\mathrm{LES}}, \tag{1}$$

where f_I represents the interface function. Interface-type models commonly solve URANS equations in attached boundary layer regions and switch to an LES-type model everywhere else, aiming at including all massively separated regions. The switch between URANS and LES is often affected by the local grid resolution, thus making solutions highly sensitive to grid topology. Representative of the interface-type models are the original DES and its extended incarnations, which include delayed detached eddy simulation (DDES)[12] and improved delayed detached eddy simulation (IDDES).[13]

In blended models, the hybrid residual stress tensor is provided by modifying the URANS tensor using a multiplicative function f_B,[14] and not relying on the LES equations:

$$\tau_{ij} = f_B \tau_{ij}^{\mathrm{URANS}}. \tag{2}$$

Examples of blended models are limited numerical scales (LNS)[15] by Batten *et al.*, the partially integrated transport model (PITM)[16,17] by Chaouat and Schiestel, and the self-adapting, two-equation model of Perot and Gadebusch.[18,19]

An additional family of models uses two velocity fields to solve both URANS and LES simultaneously with one of the two models usually "driving" under specified conditions. Advancements of that concept include dual-mesh approaches solving synchronized LES and URANS simulations on two distinct grids, each one optimized for its turbulence model, with the LES grid being typically coarse near the walls.[20] In a promising recent advancement by Nguyen and co-workers,[21,22] an activation criterion detects regions in which the LES solution is under-resolved so that LES fields can be "corrected" toward URANS ones; otherwise, URANS is corrected toward LES.

The accuracy of hybrid turbulence models is typically dependent on the flow modeled. For example, in aerospace-type external flows, interfacing an LES solution in separated flow regions with a RANS solution in boundary layers has led to the successful advancement of interfaced methods such as DES and its successors. Nevertheless, it is common for hybrid models to have limited applicability outside their original validation areas, in particular for internal flow applications. General issues encountered in the literature have been large, nonphysical fluctuations of resolved fields, poor robustness, and notably inconsistent grid convergence.[23–27]

Frohlich and von Terzi[8] have further introduced the category of second-generation URANS (2G-URANS) turbulence models, which aim at extending URANS capabilities by introducing substantial resolution of turbulent fluctuations, without introducing an explicit dependency on the computational grid. Menter *et al.*[28,29] introduced the scale adaptive simulation (SAS) model, which uses the von Kármán length scale to determine the local scale of the underlying flow field. A major challenge of SAS has been reported as its accuracy in predictive simulations in which the user is unfamiliar with the flow-specific grid requirements.[24,27] Girimaji[30] proposed the partially averaged Navier–Stokes (PANS) model, which introduces damping ratios for the modeled turbulent kinetic energy (TKE) and turbulent dissipation rate (TDR) compared to the baseline URANS model. The PANS damping ratios adjust terms in the model equations to partially resolve turbulence and are given as follows:

$$f_k = \frac{k_m}{k} \quad \text{and} \quad f_\varepsilon = \frac{\varepsilon_m}{\varepsilon} \text{ with } 0 \le f_k \le f_\varepsilon \le 1, \tag{3}$$

where k_m/k and $\varepsilon_m/\varepsilon$ are the ratios of unresolved-to-total turbulent kinetic energy and turbulent dissipation rate, respectively. A valuable theoretical analysis of the LES capability of URANS equations was recently performed by Heinz in relation to PANS and PITM models.[31] The PANS concept allows for straightforward implementation into an existing URANS solver, but the specification of f_k and f_ε requires appropriate closure, for which formulations have been proposed by multiple authors.[32–34] Many of those formulations contain a grid size term, which does not qualify them to be categorized as 2G-URANS.

In the present work, a 2G-URANS turbulence model with focus on industrial robustness is described and tested in its closed form. The approach is based on the original STRUCTure-based turbulence resolution concept (STRUCT) presented by Lenci and Baglietto,[35,36] which is extended into a complete formulation ("STRUCT-Transport" or "STRUCT-T"), with the use of modeled scales determined through transport-based averaging. The model adopts as its baseline URANS a $k-\varepsilon$ anisotropic nonlinear eddy viscosity model (NLEVM) with a cubic stress–strain relation,[37] while enabling controlled scale-resolution inside flow regions where the scale separation assumption of URANS is not satisfied. The closed formulation is compared against a "controlled" version of the model that uses tuned parameters to assess the performance of the complete formulation. Finally, the model is benchmarked against canonical datasets that demonstrate common industrial flow challenges. To date, the STRUCT concept originally proposed by Lenci and Baglietto[36] has been tested by multiple authors,[38–48] who have also proposed further variants.

II. MODEL FORMULATION

The adopted closure approaches are described here, starting from the general STRUCT formulation and progressing to the details of the "controlled STRUCT" and complete STRUCT-T. Additionally, the

details of the baseline NLEVM URANS model,[37,49] and the LES closure with wall adapting local eddy viscosity (WALE),[4] are provided for completeness.

A. General STRUCT closure concept

The STRUCT closure concept was proposed by Lenci and Baglietto[36] and introduces a resolution control parameter, r, to regulate the content of the resolved field, following the original proposal of Liu and Shih.[50] In the STRUCT approach, this parameter multiplies the definition of eddy viscosity:

$$\mu_t = \rho C_\mu \frac{k_m^2}{\varepsilon} r, \tag{4}$$

and is defined as:

$$r = \begin{cases} 1, & h \leq 1, \\ \phi, & h > 1, \end{cases} \tag{5}$$

where h and ϕ are both functions of time and space. The switch function h controls the activation of hybridization over the baseline URANS, while the reduction parameter ϕ determines the magnitude of TKE reduction in regions of model activation. For the controlled STRUCT model of Sec. II B, the reduction parameter ϕ is a constant optimized *a posteriori* with the goal of obtaining activation fields informing the development and assessment of the complete model; for the complete STRUCT-T of Sec. III C, it is dynamically evaluated from the comparison of selected flow scales.

The hybridization condition h used in STRUCT is specified by the product of two working parameters describing the modeled and resolved turbulent scales, respectively:

$$h = t_m f_r, \tag{6}$$

where t_m defines a timescale for modeled turbulence according to the baseline URANS closure, and f_r is a frequency representing resolved flow scales.

The definition used for t_m is:

$$t_m \equiv \langle t_{m,0} \rangle, \tag{7}$$

where the chevrons represent an averaging operation needed to provide a smooth local value, representative of the modeled time scales, $t_{m,0}$. To determine those time scales, this work considers a baseline URANS model based on the $k-\varepsilon$ equations and therefore:

$$t_{m,0} = \frac{k_m}{\varepsilon}. \tag{8}$$

The frequency representing resolved flow scales, f_r, is defined as:

$$f_r \equiv \sqrt{|\overline{II}|}, \tag{9}$$

where the second invariant of the resolved velocity gradient tensor is defined as follows:

$$\overline{II} = -\frac{1}{2}\frac{\partial \overline{u}_i}{\partial x_j}\frac{\partial \overline{u}_j}{\partial x_i}, \tag{10}$$

and the overbar in this case indicates resolved quantities.

The selection of this parameter for the STRUCT activation allows respecting Galilean and frame rotation invariance, making it suitable for general turbulence modeling. Moreover, the second invariant of the velocity gradient tensor is used extensively in topology literature to identify coherent structures,[51] which inspires the name of the model and suggests a physical interpretation for the activation zones of the hybridization strategy. Most valuably, the parameter has the feature of being null in simple shear layers, which causes STRUCT to revert to the baseline URANS equations, and large at the rapid distortion limit for both strain and rotation of the resolved field, which activates hybridization where the fundamental URANS assumptions are violated.

B. Controlled STRUCT formulation

To evaluate the applicability of the STRUCT hybridization approach, a controlled formulation can be adopted, where the required model closure coefficients, t_m and ϕ, are obtained from precursor URANS solutions. A geometric averaging of the $t_{m,0}$ field in regions of strong flow deformation is used to perform the chevron operation of Eq. (7), while the reduction parameter ϕ is selected *a posteriori* to find an optimal limiting condition for the scale-resolving behavior. Simulation results obtained with the controlled approach provide an understanding of the behavior of STRUCT activation and enable comparison with the complete STRUCT-T formulation.

C. STRUCT-T formulation

STRUCT-T is a complete model in which all closure parameters adapt automatically to the flow. The evaluation of the reduction coefficient ϕ of Eq. (5) is based on the rationale that an increasing overlap between modeled and resolved scales requires resolution of finer scales of turbulence to provide greater model accuracy. This translates into an inverse relation between the variables ϕ and h of Eq. (5):

$$\phi = \frac{1}{h}. \tag{11}$$

Combining Eqs. (5), (6), and (11), and introducing a calibration coefficient α, the following compact relation for the resolution control parameter is obtained:

$$r = \min\left(\frac{1}{\alpha t_m f_r}, 1\right). \tag{12}$$

The coefficient α is a constant that has shown general applicability and has been optimized to the value of 1.35.[36]

To evaluate Eq. (12), an averaging operator needs to be defined for Eq. (7) and should produce a smooth field for t_m. Explicit averaging algorithms can produce smooth fields dynamically, at the cost of heavy computational overhead in parallel computations due to their non-local nature. To address the need for a computationally efficient approach, the STRUCT-T implementation uses a Lagrangian operator in the form of an additional transport equation, relying only on local values and leveraging the existing numerical approximation practices. This approach allows leveraging the optimized performance of general-purpose CFD solvers.

A similar Lagrangian method, although only propagating in time, was used by Meneveau *et al.*[52] to replace explicit filtering in dynamic LES. The operation used by Meneveau *et al.*[52] applies to a

generic field $f(\boldsymbol{x}, t)$ and yields an averaged field $\langle f \rangle_{\mathrm{T}}$ by solving the following transport equation:

$$\frac{\overline{D}\langle f \rangle_{\mathrm{T}}}{\overline{D}t} = \frac{1}{T}\left(f - \langle f \rangle_{\mathrm{T}}\right). \tag{13}$$

The rationale for this equation is that $\langle f \rangle_{\mathrm{T}}$ is the solution to the following averaging:

$$\langle f \rangle_{\mathrm{T}}(\boldsymbol{x}, t) = \int_{-\infty}^{t} f(\boldsymbol{x}, t) g_T(t - t')\mathrm{d}t'. \tag{14}$$

Assuming constant parameters, the convolution kernel g_T is a negative exponential in time following a characteristic timescale, T:

$$g_T(t - t') = T^{-1}\mathrm{e}^{-\frac{t-t'}{T}}. \tag{15}$$

As observed in Eq. (15), the operation in Eq. (13) corresponds to a weighted average of function f along the fluid's trajectory using a weight that decays exponentially backward in time. This Lagrangian approach was used by Meneveau *et al.*[52] because of the computational advantages of the formulation compared to explicit sampling.

Here, we propose adding a spatial dimension to the method proposed by Meneveau *et al.*[52] The selected operator has been discussed by Germano[53] as a promising method for differential filtering in LES but has not been adopted extensively in modeling. Considering a generic field, $f(\boldsymbol{x}, t)$, a differential Lagrangian averaging operation is defined as the solution to the following transport equation. The equation includes a length scale, L, and a timescale, T:

$$\frac{\mathrm{d}\langle f \rangle_{T,L}}{\mathrm{d}t} + \boldsymbol{u} \cdot \nabla \langle f \rangle_{T,L} = \frac{L^2}{T}\nabla^2 \langle f \rangle_{T,L} + \frac{1}{T}\left(f - \langle f \rangle_{T,L}\right). \tag{16}$$

The above transport equation is different from that in Eq. (13) since it contains a diffusion term in addition to the source term, and it depends on both time and length scales, T and L. Analogously to the time-only case, the average field $\langle f \rangle_{T,L}$ can be written as the solution to the following operation, hereby integrated in both time and space:

$$\langle f \rangle_{\mathrm{T,L}}(\boldsymbol{x}, t) = \int_{-\infty}^{t} \int_{\mathcal{R}^3} f(\boldsymbol{x}', t') g_{T,L}(\boldsymbol{x} - \boldsymbol{x}', t - t')\mathrm{d}^3\boldsymbol{x}'\mathrm{d}t'. \tag{17}$$

In the particular case of uniform and constant $\boldsymbol{u}$, T, L, the averaging kernel in the above equation corresponds to a Gaussian filter in space and a negative exponential in time:

$$g_{T,L}(\boldsymbol{x} - \boldsymbol{x}', t - t') = \frac{1}{T}\mathrm{e}^{-\frac{t-t'}{T}} \frac{1}{\left(4\pi\frac{L^2}{T}(t - t')\right)^{\frac{3}{2}}} \mathrm{e}^{-\frac{\|\boldsymbol{x}-\boldsymbol{x}'-\boldsymbol{u}(t-t')\|_{\mathrm{L}_2}^2}{4\frac{L^2}{T}(t-t')}}. \tag{18}$$

The application to the STRUCT-T model takes benefit from biasing the operator in space, thus multiplying the time scales by a small reduction factor β:

$$\frac{\mathrm{d}\langle f \rangle_{T,L}}{\mathrm{d}t} + \boldsymbol{u} \cdot \nabla \langle f \rangle_{T,D} = \frac{1}{\beta}\left(\frac{L^2}{T}\nabla^2 \langle f \rangle_{T,L} + \frac{1}{T}\left(f - \langle f \rangle_{T,L}\right)\right). \tag{19}$$

A value of 0.01 has been chosen for β because of the stable performance demonstrated in preliminary tests.[36,54] This selection corresponds to biasing the averaging mostly in space.

In practice, the model is implemented by calculating t_{m} of Eq. (7) using the following transport equation in the solver:

$$\frac{\mathrm{d}t_{\mathrm{m}}}{\mathrm{d}t} + \boldsymbol{u} \cdot \nabla t_{\mathrm{m}} = \frac{1}{\beta}\left(\frac{L^2}{T}\nabla^2 t_{\mathrm{m}} + s\right). \tag{20}$$

The characteristic time and length scales used are derived directly from the $k - \varepsilon$ model,

$$L = \sqrt{C_\mu}\frac{k_{\mathrm{m}}^{\frac{3}{2}}}{\varepsilon}, \tag{21}$$

$$T = \frac{k_{\mathrm{m}}}{\varepsilon}, \tag{22}$$

with $C_\mu = 0.09$ from the standard k–ε closure. The source term in Eq. (23) is implemented following Eq. (19) with the addition of limiters to avoid strong variations of t_{m} in complex flows within each time step, Δ_t,

$$s = \min\left(\max\left(\frac{1}{T}(t_{\mathrm{m},0} - t_{\mathrm{m}}), -\frac{2t_{\mathrm{m}}}{\Delta_t}\right), \frac{2t_{\mathrm{m}}}{\Delta_t}\right). \tag{23}$$

The use of these limiters increases the model's stability and its adaptation to initial conditions. To ensure even greater stability in complex flows, the field for t_{m} is clipped, as typically done for variables in general-purpose transport equation solvers for CFD, to use values for t_{m} restricted to a reasonable physical range in the domain. In the flow cases presented here, that range was taken between a very small number, i.e., 10^{-10} s, and 1 s.

D. URANS-NLEVM formulation

The performance of a URANS-based hybrid model depends strongly on the suitability and accurate physical representation of the baseline URANS formulation. NLEVMs can achieve measurable advantages in terms of accuracy compared to linear models while preserving low computational cost and numerical stability. Several studies in the literature suggest that hybrid models based on NLEVMs can achieve superior performance compared to the same hybrid models based on linear URANS, as anisotropy in the modeled scales affects the description of resolved scales. Gopalan and Jaiman,[14] for example, demonstrated increased accuracy of a hybrid-NLEVM on a tandem cylinder flow case compared to its hybrid-linear counterpart. Even the pioneering hybrid turbulence model proposed by Speziale[6] was based on a NLEVM rather than a linear formulation.

The baseline URANS model adopted for the STRUCT approach is the NLEVM proposed by Baglietto and Ninokata[37,49] and is based on the original proposal of Pope[55] as later formulated by Lien *et al.*[56] The model is built on the standard $k - \varepsilon$ equations as repeated in Eqs. (24) and (25), where the coefficients recommended by Launder and Spalding[57] are used as: $C_{\varepsilon 1} = 1.44$, $C_{\varepsilon 2} = 1.92$, $\sigma_k = 1.0$, *and* $\sigma_\varepsilon = 1.3$.

$$\frac{\partial k}{\partial t} + \overline{u}_j\frac{\partial k}{\partial x_j} = \frac{\partial}{\partial x_j}\left[\left(\nu + \frac{\nu_{\mathrm{t}}}{\sigma_k}\right)\frac{\partial k}{\partial x_j}\right] + P_k - \varepsilon, \tag{24}$$

$$\frac{\partial \varepsilon}{\partial t} + \overline{u}_j\frac{\partial \varepsilon}{\partial x_j} = \frac{\partial}{\partial x_j}\left[\left(\nu + \frac{\nu_{\mathrm{t}}}{\sigma_k}\right)\frac{\partial \varepsilon}{\partial x_j}\right] + C_{\varepsilon 1}\frac{\varepsilon}{k}P_k - C_{\varepsilon 2}\frac{\varepsilon^2}{k}. \tag{25}$$

The standard production term is used for turbulent kinetic energy:

$$P_k = -\tau_{ij}\frac{\partial \overline{u}_i}{\partial x_j}. \tag{26}$$

Linear models rely on the Boussinesq[58] method, modeling the unknown terms, i.e., the Reynolds stresses τ_{ij}, with a linear proportionality between residual anisotropic stresses and strains in the resolved flow field:

$$\tau_{ij} = \frac{2}{3}k\delta_{ij} - 2\nu_t\overline{S}_{ij}, \tag{27}$$

where according to the standard $k-\varepsilon$ model, the turbulent eddy viscosity, ν_t, is defined as:

$$\nu_t = C_\mu\frac{k^2}{\varepsilon}. \tag{28}$$

This simple relation is notably unsuitable for the description of complex strain and leads to inaccurate predictions in flows where curvature, rotation, stagnation, or secondary flows are present. Pope[55] proposed a NLEVM formulation as an explicit algebraic simplification of the exact stress–strain relation. Residual anisotropic stresses in this formulation are described by a polynomial formulation which is a function of k, ε, and various invariants derived from the resolved velocity gradient tensor.

The selected formulation was specifically extended to provide general robustness and advanced description of anisotropy when applied to industrial internal flows.[59,60] In this model, the residual stress anisotropy tensor is defined as follows:

$$\begin{aligned} a_{ij} &= \tau_{ij} - \frac{2}{3}k\delta_{ij} = \nu_t\left(-2\overline{S}_{ij} + q_{ij} + c_{ij}\right) \\ &= -2\nu_t\overline{S}_{ij} + 4C_1\nu_t\frac{k}{\varepsilon}\left[\overline{S}_{ik}\overline{S}_{kj} - \frac{1}{3}\delta_{ij}\overline{S}_{kl}\overline{S}_{kl}\right] \\ &\quad + 4C_2\nu_t\frac{k}{\varepsilon}\left[\overline{\Omega}_{ik}\overline{S}_{kj} + \overline{\Omega}_{ik}\overline{S}_{kl}\right] \\ &\quad + 4C_3\nu_t\frac{k}{\varepsilon}\left[\overline{\Omega}_{ik}\overline{\Omega}_{jk} - \frac{1}{3}\delta_{ij}\overline{\Omega}_{kl}\overline{\Omega}_{jk}\right] \\ &\quad + 8C_4\nu_t\frac{k^2}{\varepsilon^2}\left[\overline{S}_{ki}\overline{\Omega}_{ij} + \overline{S}_{kj}\overline{\Omega}_{li}\right]\overline{S}_{kl} \\ &\quad + 8C_5\nu_t\frac{k^2}{\varepsilon^2}\left[\overline{S}_{kl}\overline{S}_{kl} - \overline{\Omega}_{kl}\overline{\Omega}_{kl}\right]\overline{S}_{ij}, \end{aligned} \tag{29}$$

where q_{ij} and c_{ij} are the quadratic and cubic tensors extending the linear model. Equations (30) and (31) describe the resolved strain and rotation in both dimensional and dimensionless forms

$$\overline{S}_{ij} = \frac{1}{2}(\overline{u}_{ij} + \overline{u}_{ji}),\ \overline{\Omega}_{ij} = \frac{1}{2}(\overline{u}_{ij} - \overline{u}_{ji}), \tag{30}$$

$$\overline{S}^* = \frac{k}{\varepsilon}\sqrt{2\overline{S}_{ij}\overline{S}_{ij}},\ \overline{\Omega}^* = \frac{k}{\varepsilon}\sqrt{2\overline{\Omega}_{ij}\overline{\Omega}_{ij}}. \tag{31}$$

The non-constant coefficients used here are as follows:

$$C_\mu = \frac{C_{a0}}{C_{a1} + C_{a2}\overline{S}^* + C_{a3}\overline{\Omega}^*}, \tag{32}$$

$$C_1 = \frac{C_{NL1}}{\left(C_{NL6} + C_{NL7}\overline{S}^{*3}\right)C_\mu}, \tag{33}$$

$$C_2 = \frac{C_{NL2}}{\left(C_{NL6} + C_{NL7}\overline{S}^{*3}\right)C_\mu}, \tag{34}$$

$$C_3 = \frac{C_{NL3}}{\left(C_{NL6} + C_{NL7}\overline{S}^{*3}\right)C_\mu}, \tag{35}$$

$$C_4 = C_{NL4}C_\mu^2, \tag{36}$$

$$C_5 = C_{NL5}C_\mu^2. \tag{37}$$

The model constants used in the above formulations are adapted from the literature[37,49] and reported in Table I.

E. A comment on the defensive strategy

STRUCT can be categorized as a 2G-URANS approach that aims at dynamically determining flow regions where scale-resolving modeling is most needed, reverting to the baseline URANS otherwise. All STRUCT implementations rely on the baseline URANS in regions of undisturbed flow even if the local grid would justify the use of some partial scale resolution. Indeed, in mainly undisturbed flow regions, NLEVM-URANS models deliver an accurate statistical description of flow quantities. The rationale for this "defensive" strategy is to enhance the model's robustness in complex flows, seeking greater model reliability in predictive applications. The approach aims at limiting a typical side-effect of hybrid models of over-resolving scales, which often results in a shift from an accurate solution to an unphysical model error being much larger than that expected from the baseline URANS.[23–27]

F. LES-WALE formulation

The LES solutions presented in this work adopt the WALE subgrid scale (SGS) closure introduced by Nicoud and Ducros.[4] The closure models the eddy viscosity considering both the resolved strain and rotation rate and achieves a null eddy viscosity at the wall without requiring a dynamic method.

III. RESULTS AND DISCUSSION

Both the controlled STRUCT and STRUCT-T models were implemented into a numerical solver and tested on three selected flow cases, i.e., flow past a square cylinder, turbulent mixing in a T-junction, and flow through an asymmetric diffuser. The selected test cases are representative of fundamental flow configurations that appear in most complex industrial flows: massive separation, thermal cycling, and mild separation. Test case and simulation details are summarized in Table II while grid sensitivity results are reported in separate work.[36] Experimental data for validation are provided in the form of time average, variance, and covariance of velocity components. Velocity variances and covariances are presented as the sum of variances or covariances of resolved variables and time averages of respective residual stress tensor components, thus neglecting mixed terms.

A. Numerical solver

Due to the industrial focus of the STRUCT approach, all results in this work are obtained using the general-purpose commercial CFD software STAR-CCM+. A development build of the software version 7.02 had been initially leveraged to implement the necessary

TABLE I. NLEVM model constants.[37]

Coefficients	C_{a0}	C_{a1}	C_{a2}	C_{a3}	C_{NL1}	C_{NL2}	C_{NL3}	C_{NL4}	C_{NL5}	C_{NL6}	C_{NL7}
Value	0.667	3.9	1.0	0.0	0.8	11.0	4.5	−5.0	−4.5	1000.0	1.0

TABLE II. Setup of validation test cases.

	Flow past a square cylinder	Mixing in a T-junction	Asymmetric diffuser flow
Main flow phenomenon	Massive separation	Thermal cycling, thermal fatigue	Mild separation
Experimental data	Lyn *et al.*[61]	Smith *et al.*[62]	Buice[63]
Measurement technique	Laser Doppler velocimetry	Particle image velocimetry	Hot-wire anemometry
Main cell size (mm)	10.5	4.5	1.5
Number of cells ($\times 10^6$)	0.65	0.75	1.8
Mesh type	Hexahedral	Hexahedral	Hexahedral
Wall-resolved boundaries	Cylinder walls	None	Top and bottom walls
Wall-modeled boundaries	Top and bottom walls	All walls	None
Periodic boundaries	Spanwise direction	Spanwise direction	Spanwise direction
t_m for controlled STRUCT (s)	0.33	0.1	0.01
r for controlled STRUCT (-)	1×10^{-10}	0.6	0.6

reductions parameter, a feature that has become standard in recent code versions. In the finite volume solver, the segregated pressure–velocity solution is used, based on the semi-implicit method for pressure-linked equation (SIMPLE) algorithm,[64] and adopting the Rhie–Chow interpolation[65] to prevent numerical oscillations affecting the solution. Typical choices for under-relaxation factors are made: 0.7 for velocity, 0.3 for pressure, and 0.8 for both the turbulent kinetic energy and turbulent dissipation rate equations. To approximate the convective terms, a second-order nanoscillatory upwind scheme is adopted for the URANS simulations. A hybrid Gauss-least squares method is used for computing gradients, with Venkatakrishnan's reconstruction gradient limiter. For LES and STRUCT solutions, a second-order central scheme is used with 5% boundedness (of second-order upwind scheme), where boundness is introduced only when the local Normalized-Variable Diagram (NVD) value is outside the range 0–1. Time integration is achieved with a second-order accurate three-time level backward Euler method. Time steps sizes are selected to enforce a maximum Courant number around 1. For URANS, only NLEVM results are shown, while separate work[36] has demonstrated a consistently increased accuracy for the adopted NLEVM in comparison to the standard k–ε closure.

B. Flow past a square cylinder

The first test case examined is the flow past a square cylinder of Lyn *et al.*,[61] which represents a classic example of a confined flow interacting with an obstacle and producing a shedding trail. The flow interaction with the obstacle causes massive separation and large vortex structures that, when solved using URANS models, results in a violation of the underlying scale separation assumption. This consideration and the clear-cut distinction between regions of massive flow separation and developed flow regions make this configuration a useful "entry-level" test case for hybrid turbulence models.

In the simulation domain, a fully developed flow of water runs through a $20 \times 56\,\text{cm}^2$ channel crossed by a square cylinder of side length, $D = 4$ cm, as illustrated in Fig. 1. The reference velocity upstream the cylinder, U_{ref}, is 0.5435 m/s. The Reynolds number based on side length is 21 400. A hexahedral mesh with 650 000 cells is used with refinements around and past the obstacle and further refinements at the obstacle walls. As described in Table II and Fig. 2, a hexahedral mesh is used with a base size of 10.5 mm refined by 50% around and immediately after the cylinder. Preliminary tests have shown appropriate URANS convergence on this grid.[36]

Closure parameters for controlled STRUCT simulations are determined as discussed in Sec. II B. Values for $t_{m,0}$ are derived from a cubic URANS simulation as shown in Fig. 3. Geometric averaging of $t_{m,0}$ in the region around the square cylinder leads to the value used here of $t_m = 0.33$ s. Additional precision for such a value is not needed, because the results are insensitive to variations within 10%. A reduction coefficient close to zero is selected for optimal predictions in model activation regions: $\phi = 1 \times 10^{-10}$.[36]

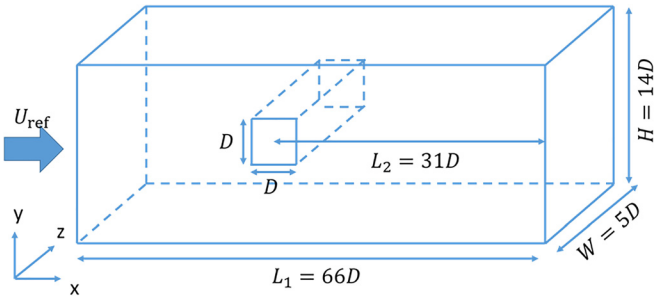

FIG. 1. Square cylinder test case simulation domain.

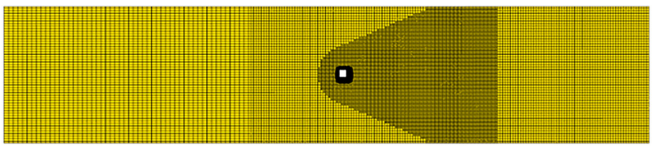

FIG. 2. Mesh configuration for the square cylinder test case.

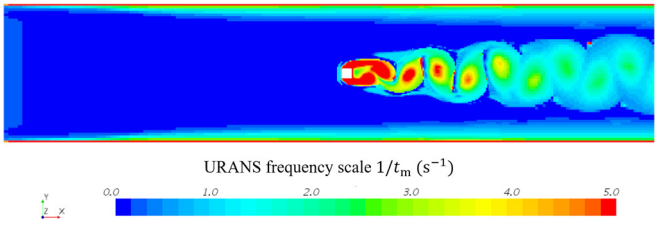

FIG. 3. Cubic URANS results used for determining the activation conditions.

The complete STRUCT-T formulation uses a transport equation to automatically calculate the resolution control parameter, r [Eq. (12)]. Figure 4 shows activation regions of the controlled STRUCT and STRUCT-T models for the test case. The red color represents regions where the baseline URANS equations are solved and the STRUCT concept expects scale separation to occur. Both STRUCT models decrease the resolution control parameter in regions around and past the square cylinder, where significant flow deformation is expected. As expected, the STRUCT-T model performs this reduction with an automatic, continuous, and smooth function, as opposed to the binary mode of the controlled STRUCT model, which is driven by controlled parameters.

Figure 5 compares snapshots of resolved velocity distribution contours obtained with different turbulence models. URANS results appear to only describe low-frequency evolutions of shedding while

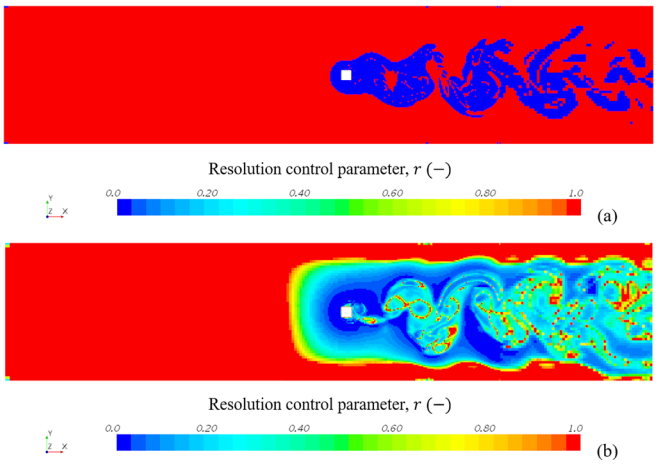

FIG. 4. Activation regions of the STRUCT models in the square cylinder test case. (a) and (b) represent results from controlled STRUCT and STRUCT-T model, respectively.

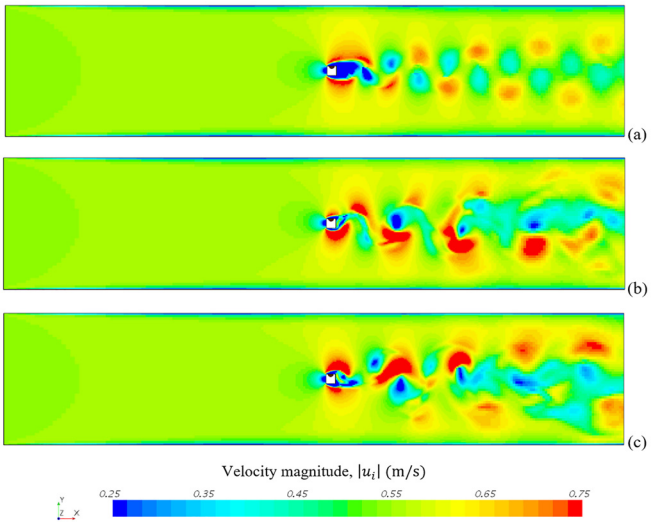

FIG. 5. Instantaneous velocity fields for different turbulence models in the square cylinder test case. Results are shown for (a) URANS, (b) controlled STRUCT, and (c) STRUCT-T models, respectively.

both the controlled STRUCT and STRUCT-T models capture a broader spectrum of shedding fluctuations.

Profiles for the first and second moments of velocity components along with time (i.e., velocity mean, variance, and covariance) are shown in Fig. 6. The figure compares experimental data points with velocity profiles from the baseline cubic URANS, controlled STRUCT, and STRUCT-T models. URANS results are in weak agreement with the experiment, with a greater deviation in the region around and downstream the obstacle. For example, URANS strongly underpredicts the x component of velocity around position $2D$ past the obstacle. Furthermore, the URANS model fails to predict velocity variance profiles in the same regions, where the flow, disturbed by the obstacle, produces a significant amplitude of velocity fluctuations in the experimental data. Conversely, a generally closer agreement with the experiment is observed for the controlled STRUCT and STRUCT-T models. However, the models slightly overpredict the x component of velocity around position $2D$ past the obstacle, still being much closer to experimental values compared to the strong underprediction by URANS. The benefits of STRUCT, as opposed to the baseline cubic URANS, appear to be stronger in regions near the obstacle, where massive separation takes place, in regions in and after the wake, and in regions where strong shedding occurs.

The favorable results obtained by the controlled STRUCT approach with a very low value of ϕ indicate that this is an "easy" test case for hybrid turbulent models as increased hybridization results in greater model accuracy. Two increasingly challenging test cases are discussed next.

C. Turbulent mixing in a T-junction

The simulation of thermal mixing in a T-junction is an industrially relevant test case characterized by hot and cold flow streams mixing and producing turbulence-induced temperature fluctuations at the piping wall. These fluctuations generate cyclic thermal stresses that

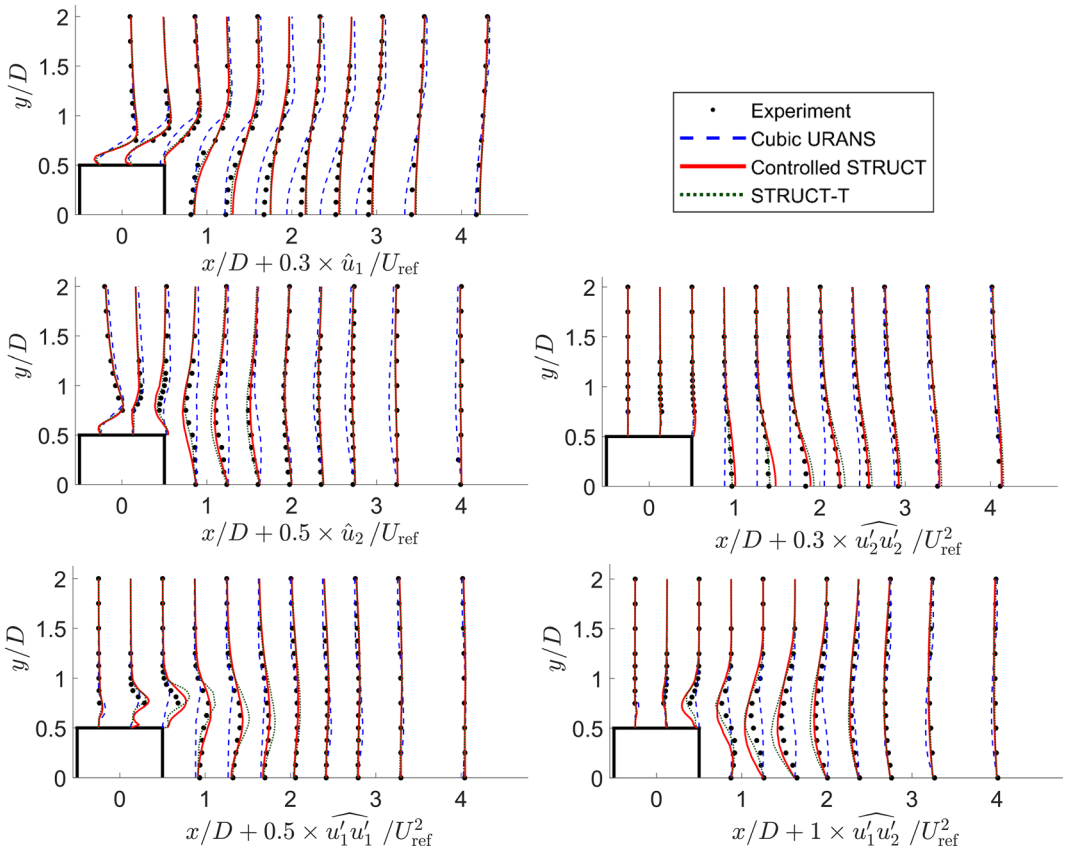

FIG. 6. Square cylinder test case: mean, variance, and covariance of velocity components compared between simulation results and experimental data.

can lead to thermal fatigue cracking of the wall material.[66] Unlike the square cylinder test case, the T-junction does not have a well-defined URANS failure region, representing thus a challenging scenario for hybrid models.[27] The Vattenfall T-junction experiment is used here due to its pedigree and the documented failure of existing hybrid closures.[27] In the experiment, cold (19 °C) water flowing through a 140 mm diameter pipe encounters an intersection where warm (36 °C) water is injected through a smaller (100 mm) diameter pipe; the volumetric flow rates are 9×10^{-3} and 6×10^{-3} m^3/s for the cold and hot flow, respectively. Schematics of the thermal mixing in T-junction are shown in Fig. 7. Experimental acquisitions[27] include laser-Doppler velocimetry (LDV), particle image velocimetry (PIV), and temperature measurements made with thermocouples. The velocity measurements provided for benchmarking were acquired using PIV.

Similarly to the approach discussed in Sec. III C, a preliminary cubic URANS simulation is run to obtain instantaneous values for $t_{\mathrm{m},0}$ as needed to inform the controlled STRUCT model. Geometric averaging of $t_{\mathrm{m},0}$ around the location of interest leads to a value of modeled timescale of 0.1 s. A suitable value for ϕ has been determined *a posteriori* as 0.6.[36]

Activation regions resulting from the controlled STRUCT and STRUCT-T models for this test case are shown in Fig. 8. The figure shows that the hybrid model is only activated in regions that are qualitatively expected to contain most of the disturbed flow features: those at and downstream of the junction. Small regions of model activation are observed near the two inlets for STRUCT-T. This effect is due to the adaptation of the flow to the imperfect description of velocity and turbulent profiles at the inlet boundary.

For this test case, in addition to URANS and STRUCT simulations, an LES result was obtained on a grid with 23 times more cells compared to the mesh used for URANS and STRUCT. The number of cells used for LES, 17 million, is consistent with the number of cell range of the three submissions with the top velocity score in the Vattenfall benchmark[27] (i.e., 70.5, 34, and 13.2 $\times$ 10^6 cells).

Figure 9 shows snapshots of resolved velocity contours. Cold streamlines from the branch pipe reach the junction and travel for a

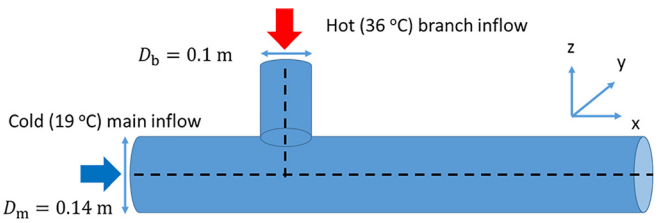

FIG. 7. Vattenfall T-junction simulation domain.

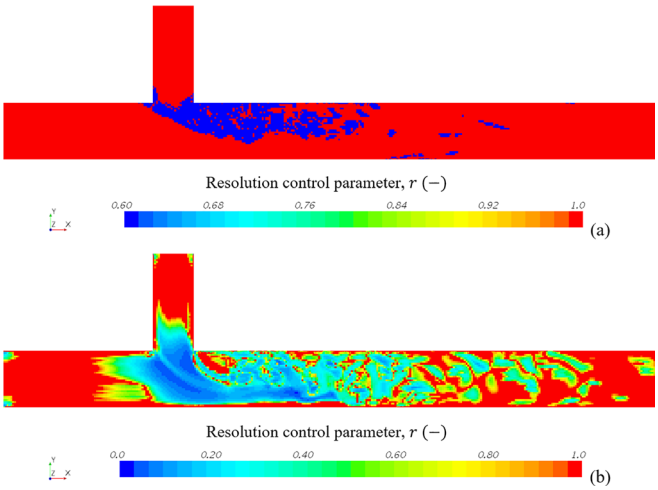

FIG. 8. Activation regions of the STRUCT models in the T-junction test case. (a) and (b) represent the results from controlled STRUCT and STRUCT-T models, respectively.

short distance before being deflected downstream by the oncoming hot flow. A stratified layer forms from the trailing edge of the branch pipe toward the bottom wall, and the entry of the hot inflow results in flow separation and recirculation zones near the edges of the junction. The LES model describes the flow separation and vortex shedding phenomena, while the URANS model, as expected, does not reproduce the unsteady complex shedding observed through LES, predicting an overly stratified flow configuration. Despite adopting the same mesh as for the URANS solution, both the controlled STRUCT and STRUCT-T models introduce local resolution of the turbulent scales in areas at, and past, the junction and are able to reproduce the qualitative trend of large unsteady turbulent structures observed in the LES results. The finest scales observed in LES are not resolved in STRUCT, providing an example of the model's strategy, for which robustness is valued more than seeking full LES behavior, aiming at a coarse-grid extension of URANS capabilities.

The qualitative description of turbulent coherent structures can be analyzed by presenting isosurfaces of the Q-criterion, as shown in Fig. 10. The boundary layer separation induced by the adverse pressure gradient and the high shear interface between the two jet streams, as the branch inflow mixes with the main inflow, generate large flow structures. These structures extend in the streamwise direction and gradually disappear as they decay into finer isotropic turbulence. The shape of the turbulent structures observed for LES and the two STRUCT models is mutually consistent, where the STRUCT approaches mostly resolve the large structures while modeling further decayed regions. The URANS model clearly overestimates the turbulent eddy viscosity in the high shear region, therefore immediately damping the structures downstream of the mixing tee and failing to reproduce the large unsteady mixing.

Figure 11 compares the dimensionless mean, variance, and covariance of velocity profiles from the different turbulence models with experimental data.[27] The figure shows mean

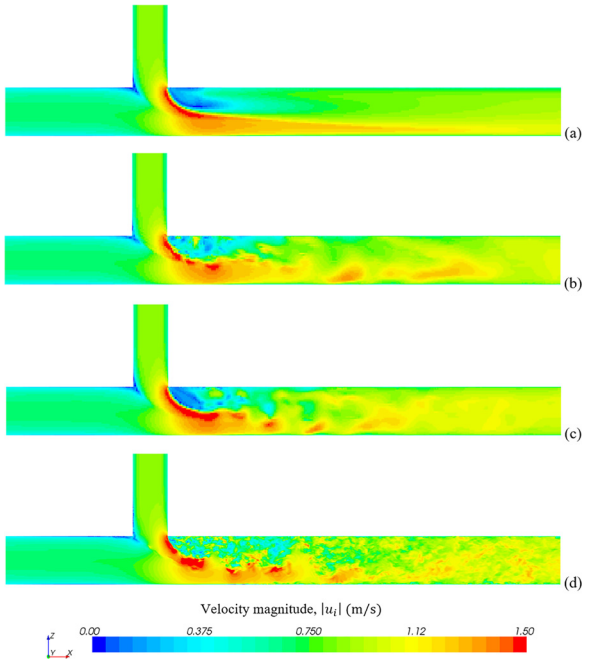

FIG. 9. Instantaneous velocity fields for different turbulence models in the T-junction test case. (a)–(d) represent the results from URANS, controlled STRUCT, STRUCT-T, and LES models, respectively.

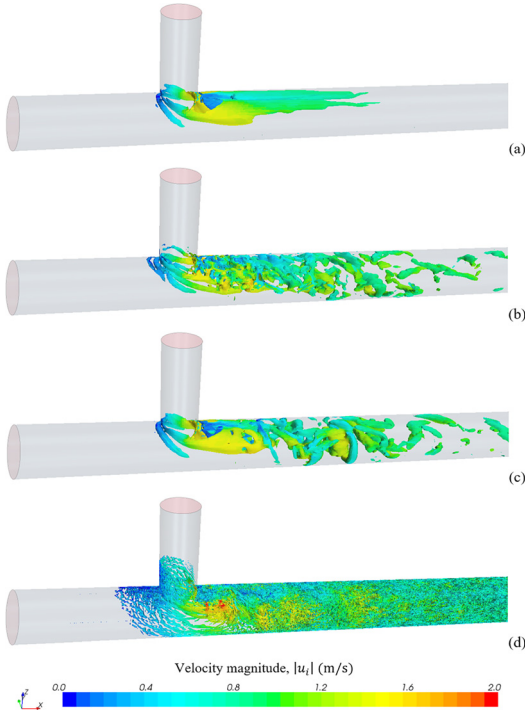

FIG. 10. Comparison of turbulent structures (Q-criterion contours with value of 50 s^{-2}) for URANS (a), controlled STRUCT (b), STRUCT-T (c), and LES (d) models. Isosurfaces are colored by velocity.

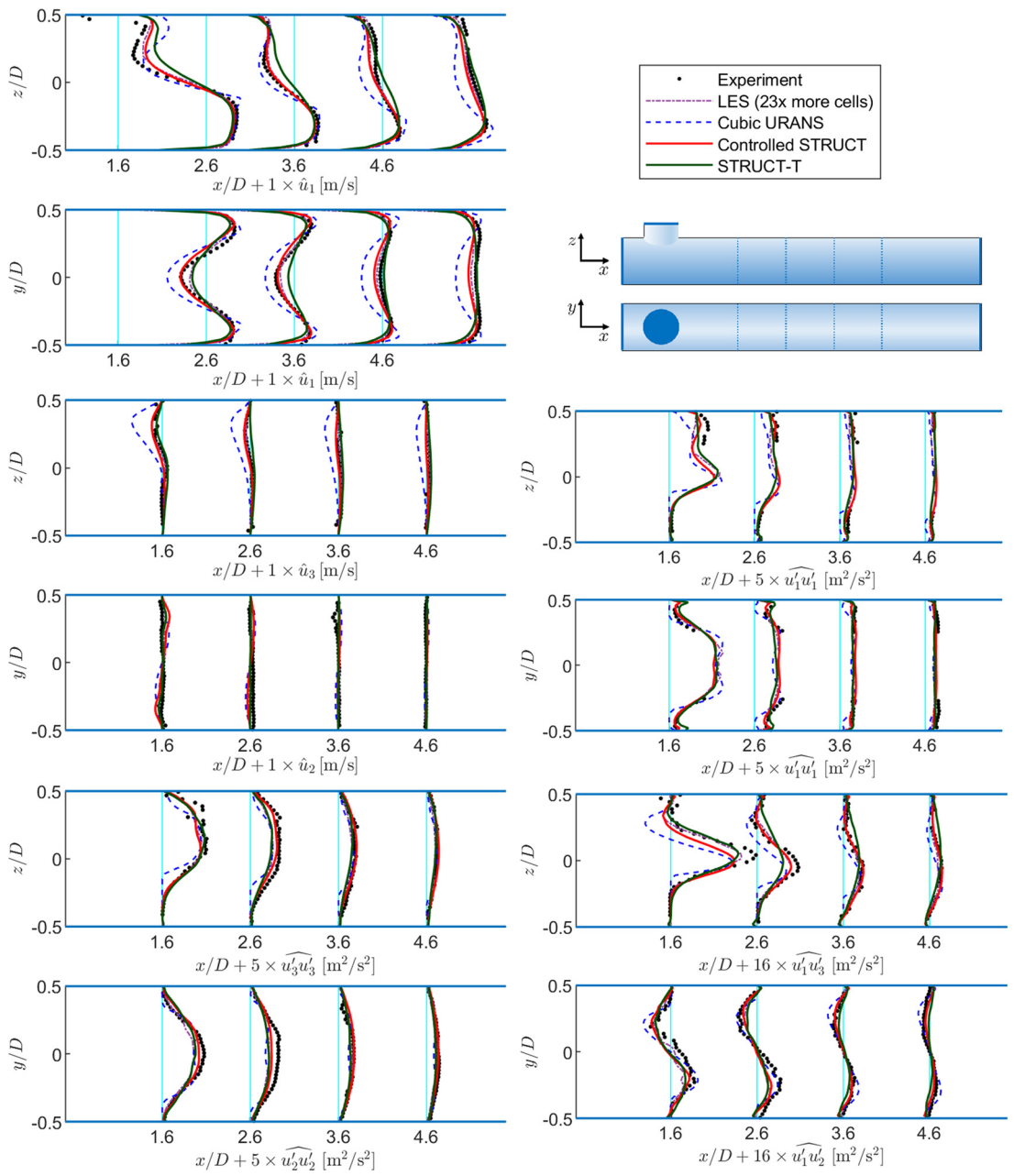

FIG. 11. T-junction test case: mean, variance, and covariance of velocity components compared between simulation results and experimental data.

velocities from STRUCT and LES agreeing closely with the experiment. On the other hand, URANS profiles underestimate velocities strongly near the center of the pipe in the most downstream locations, compensating with higher values near the pipe walls along the horizontal plane. This behavior can be interpreted as the effect of excessive eddy viscosity predicted by the model in the mixing region.

Figure 11 also compares variances and covariances of velocity components. The experimental report from the Vattenfall tests notes a large systematic uncertainty near the center of the pipe for $\widehat{u_1'u_1'}$, due to reflection of the PIV light sheet on the tube wall.[62] Those experimental values are omitted near the domain center in Fig. 11. Overall, LES and STRUCT results are in close agreement with each other and generally closer to the experiment than URANS results.

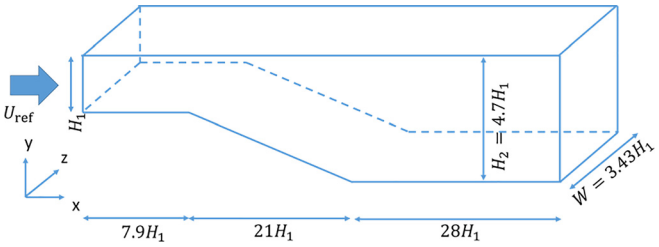

FIG. 12. Asymmetric diffuser simulation domain.

D. Flow through an asymmetric diffuser

The test case for flow through an asymmetric diffuser has been used widely to evaluate the performance of turbulence models when facing mild adverse pressure gradients. This test case has shown to be challenging for hybrid models due to the mild nature of the flow separation as opposed to the strong mixing experienced in the two test cases discussed previously; spurious hybrid activation leads to large deviations from experimental results compared to URANS.[23]

Accurate modeling of the phenomenon of flow separation is key to many engineering applications. However, the conditions producing separation typically violate the equilibrium assumption on which basic URANS models are formulated, causing predictions in poor agreement with experimental data. URANS models that are capable of predicting the location of the recirculation region are often not able to provide an accurate description of the flow in the surrounding domain.[67]

The simulation domain used here reproduces the flow as in the experimental data by Buice[63] using a fully developed air flow entering a 0.015 m tall rectangular duct. The Reynolds number is 20 000 based on the height of the inlet channel ($H_1 = 0.015$ m) and the bulk inlet velocity ($U_{ref} = 18.32$ m/s). In the diffuser section, the bottom wall has a slope with an angle of about 10°. Such a wall reverts to being horizontal where the flow domain height becomes greater than 4.7 times the inlet height. The geometry of the simulation domain is shown in Fig. 12. Experimental data used in this work were collected by Buice[63] using hot-wire anemometry, including cross-wire techniques and pulsed-wire anemometry.

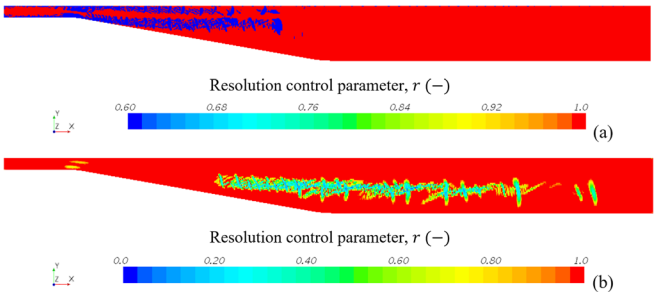

FIG. 13. Activation regions of the STRUCT models in the asymmetric diffuser test case. (a) and (b) represent the results from controlled STRUCT and STRUCT-T models, respectively.

Correspondingly to the two previous cases, a preliminary cubic URANS simulation is used to obtain instantaneous values for $t_{m,0}$; geometric averaging around the location of interest yields a value of $t_m = 0.01$ s while the value for ϕ is determined *a posteriori* as 0.6.[36]

The STRUCT activation regions for this test case are shown in Fig. 13. As expected, the hybrid models are activated in locations where significant flow deformation occurs. In particular, activation occurs near the sudden expansion. An undesired near-wall model activation is observed for the controlled STRUCT. This activation provides an example of intrinsic limitations of the controlled model, for which t_m is constant in the whole domain. Having this parameter constant is not optimal for the diffuser test case, which undergoes a significant change in turbulent scales between the inlet and outlet. The STRUCT-T model uses automatic adaptation of model scales, based on local flow variables, and overcomes this undesired inlet effect.

Figure 14 compares the velocity field distribution for different turbulence models. As expected, the URANS model fails to predict the recirculation zone caused by the mild separation. In Figs. 14(b) and 14(c),

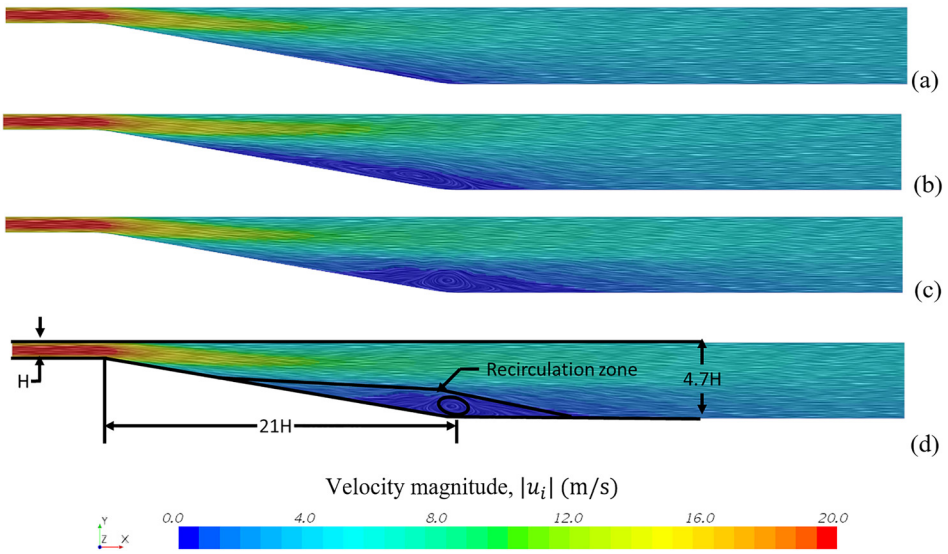

FIG. 14. Instantaneous velocity fields for different turbulence models in the asymmetric diffuser test case. (a)–(c) represent the results from URANS, controlled STRUCT, and STRUCT-T models, while (d) shows a drawing of the experimental recirculation zone by Buice[63] superimposed over (c).

a clear recirculation region forms in the bottom corner for both the controlled STRUCT and STRUCT-T models. The domain and shape of this recirculation are in good agreement with the experimental findings,[63] which are represented as black lines in Fig. 14(d).

Profiles for velocity means, variances, and covariances are plotted in Fig. 15. Values in the lower part of the domain are not provided by the authors of the experiment for the last two subplots, because measurement conditions exceeded the uncertainty limit for reliable acquisitions using the cross-wire technique.[63] The locations near the inlet and outlet are predicted similarly by all the models and are fairly close to the experimental values; this is consistent with such locations being mostly undisturbed by the unsteady flow separation. Conversely, in the central part of the plot, the STRUCT solution is much closer to experimental data than the URANS one. The URANS solution does not predict any recirculation and displays low velocity gradients, which is most likely due to an overestimate of eddy viscosity in disturbed regions. Among the models tested, the STRUCT model, especially STRUCT-T, appears to be in closer agreement with the experiment.

E. Discussion of results

The results presented for three relevant test cases provide a demonstration of the dynamic nature of the STRUCT approach and its ability to operate robustly in challenging scenarios with mild and sharp spatial variations of scale separation. In all flow cases tested, the STRUCT model achieves closer agreement with experimental measurements thanks to its local activation, which results in increased resolution of local flow structures and ultimately improved predictions of both velocity profiles and higher moments in comparison to the baseline URANS approach. By employing a continuous variable to assign the TKE ratio locally in hybrid activation regions, the STRUCT-T model achieves completeness while maintaining accuracy in challenging scenarios such as the T-junction and the asymmetric diffuser.

A fundamental aspect of the hybrid turbulence model is the balance between accurate flow description and low computational cost. In Table III, the computational cost for both STRUCT formulations is compared to that of the baseline URANS model. The comparison is based on runtime with identical simulation conditions including computational grid, time step, and boundary conditions (see Table II).

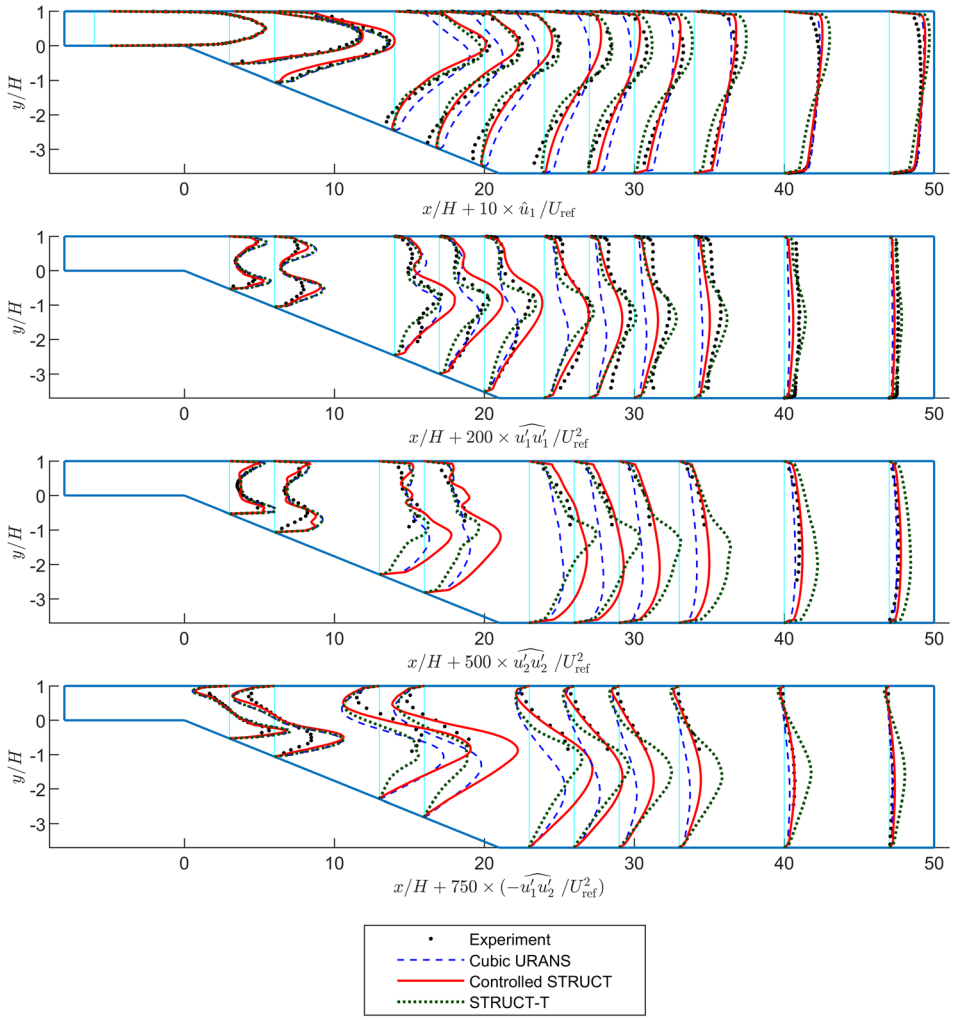

FIG. 15. Asymmetric diffuser test case: mean, variance, and covariance of velocity components compared between simulation results and experimental data.

TABLE III. Computational costs compared to the baseline URANS performance.

	Flow past a square cylinder	Mixing in a T-junction	Asymmetric diffuser flow	Average
Controlled STRUCT	14%	3%	7%	8%
STRUCT-T	24%	11%	23%	19%

As shown in Table III, the controlled STRUCT approach introduces a moderate increase in computational cost compared to URANS—by 8%, on average. This figure rises to 19% for STRUCT-T due to the need to evaluate an additional transport equation for t_m. The maximum observed increase in computational cost is 23%, which is negligible when compared to the increase required by LES, which is two orders of magnitude for the T-junction case.

The controlled STRUCT approach requires precursor URANS and STRUCT simulations, which add computational cost over the values in Table III. This cost is however not analyzed in detail as the approach is presented solely to support the evaluation of the hybridization regions and the performance of the STRUCT-T formulation.

A deliberate choice was made in the STRUCT development to only rely on parameters being local to each computational cell, in order to ensure straightforward and efficient parallel implementation. Furthermore, the transport equation in Eq. (20) has the same structure as the transport equations solved by the baseline URANS formulation. As a result, parallel scaling has shown to be unchanged from that of the baseline URANS performance of the CFD solver. The ∼19% increase in computational cost reported for STRUCT-T over URANS does not vary substantially with the grid size or parallel scaling.

IV. CONCLUSIONS

This work has demonstrated a novel hybrid turbulence modeling strategy that can be classified as second-generation URANS. The approach enables scale-resolving capability through the comparison between flow variables representing scales associated with resolved and modeled turbulence. This choice allows the hybrid behavior to be activated in regions with significant scale separation or with rapid distortion while maintaining robust URANS equations in simple shear regions. The parameter identified for describing resolved turbulence is the square root of the absolute value of the second invariant of the resolved velocity gradient tensor. It is noted that such an invariant has also been used extensively to identify coherent turbulent structures. The approach is named STRUCT to indicate a STRUCTure-based turbulence model.

A reference controlled implementation of the STRUCT model and a complete STRUCT-T formulation are tested on three relevant flow cases and compared with experimental data. The controlled STRUCT model uses case-dependent parameters selected *a posteriori* and is kept constant in the entire flow region, with the purpose of defining an optimized solution for comparison with the STRUCT-T model. The STRUCT-T closure instead does not rely on preassigned parameters but adopts a differential Lagrangian averaging operator to obtain a smooth working parameter representative of local flow fields. Results from the STRUCT models are in close agreement with experimental data for all three test cases, while adopting URANS-like meshes. The average computational cost increase compared to the baseline URANS is 8% and 19%, respectively, for the controlled STRUCT and STRUCT-T model.

Having demonstrated the robust applicability of the STRUCTure-based turbulence strategy, future work will focus on the application of the STRUCT model on a growing set of test cases, extending its assessment on external flow applications, and further aiming at simplifying the hybridization strategy.

ACKNOWLEDGMENTS

The authors owe deep gratitude to sources that have funded parts of this project over multiple years: TerraPower, the U.S. Department of Energy, Skoltech, Framatome, and the Theos J. Thompson Memorial Fellowship. Many thanks to Sylvain Lardeau for providing early access to features of the code STAR-CCM+ that allowed modifying the turbulence model. The authors are also grateful to the following people for inspiring and supporting this work with helpful research discussions and inputs: Rami Abi Akl, Michael J. Acton, Davide Concu, Pablo P. Ducru, and Jingyong Zhang.

AUTHOR DECLARATIONS

Conflict of Interest

The authors declare that there is no conflict of interest related to this work.

NOMENCLATURE

Acronyms and abbreviations

CFD	Computational fluid dynamics
DDES	Delayed detached-eddy simulation
DES	Detached-eddy simulation
DNS	Direct numerical simulation
FFT	Fast Fourier transform
IDDES	Improved delayed detached-eddy simulation
LES	Large-eddy simulation
LNS	Limited numerical scales
NLEVM	Nonlinear eddy-viscosity model
PANS	Partially averaged Navier–Stokes
PITM	Partially integrated transport model
PRNS	Partially resolved numerical simulation
RANS	Reynolds-averaged Navier–Stokes
RMS	Root-mean-square
SAS	Scale adaptive simulation
SGS	Subgrid scale model
SIMPLE	Semi-implicit method for pressure-linked equations
STRUCT	Structure-based resolution of turbulence
STRUCT-T	STRUCT-Transport formulation

TDR	Turbulent dissipation rate
TKE	Turbulent kinetic energy
URANS	Unsteady Reynolds-averaged Navier–Stokes
VLES	Very-large-eddy simulation
WALE	Wall-adapting local eddy viscosity
2G	Second generation

Latin

a_{ij}	Residual stress anisotropy tensor (J/kg)
c_{ij}	Cubic tensors in non-linear eddy viscosity model (s^{-1})
C_1, C_2, C_3, C_4, C_5, C_{NL1}, C_{NL2}, C_{NL3}, C_{NL4}, C_{NL5}, C_{NL6}, C_{NL7}	Coefficients in non-linear eddy viscosity model (-)
C_μ, $C_{\varepsilon 1}$, $C_{\varepsilon 2}$, σ_k, σ_ε	Coefficients in $k-\varepsilon$ model (-)
D, H, L, W	Generic distance, length scale, or integral length scale (m)
f, g	Generic function
f_B	Multiplicative function in blended hybrid turbulence model (-)
f_ε	PANS resolution control for ε (-)
f_I	Interface function in interfaced hybrid turbulence model (-)
f_k	PANS resolution control for k (-)
f_r	Resolved scale in STRUCT model (-)
h	Activation parameter (-)
II	Second invariant of the velocity gradient tensor (s^{-2})
k	Turbulent kinetic energy (J/kg)
k_m	Modeled turbulent kinetic energy (J/kg)
P_k	Turbulent kinetic energy production (W/kg)
q_{ij}	Quadratic tensors in non-linear eddy viscosity model (s^{-1})
Re	Reynolds number (-)
r	Ratio of resolved-to-total turbulent kinetic energy (-)
s	Source term in STRUCT-T model (-)
S_{ij}	Rate of strain tensor (s^{-1})
t	Time (s)
$t_{m,0}$	Modeled time scale in STRUCT (s)
t_m	Averaged modeled time scale in STRUCT (s)
T	Generic time scale or integral time scale (s)
U_{ref}	Reference velocity (m/s)
u_i	Velocity vector (m/s)
x_i	Position vector (m)

Greek

α	Coefficient (-)
β	Coefficient (-)
δ_{ij}	Kronecker delta
Δ_t	Time step (s)
ε	Turbulent dissipation rate (W/kg)
μ	Dynamic molecular viscosity (Pa·s)
μ_t	Dynamic eddy viscosity (Pa·s)
ν	Kinematic molecular viscosity (m^2/s)
ν_t	Kinematic eddy viscosity (m^2/s)
ρ	Density (kg/m^3)
τ_{ij}	Stress tensor, or residual stress tensor (J/kg)
ϕ	STRUCT reduction function (-)
Ω_{ij}	Rate of rotation tensor (s^{-1})

DATA AVAILABILITY

The data that support the findings of this study are available from the corresponding author upon reasonable request.

REFERENCES

[1]P. Moin and K. Mahesh, "Direct numerical simulation: A tool in turbulence research," Annu. Rev. Fluid Mech. **30**, 539–578 (1998).
[2]J. Smagorinsky, "General circulation experiments with the primitive equations: I. The basic experiment," Mon. Weather Rev **91**, 99–164 (1963).
[3]D. K. Lilly, "The representation of small scale turbulence in numerical simulation experiments," *Proceedings of the IBM Scientific Computing Symposium on Environmental Sciences* (1967).
[4]F. Nicoud and F. Ducros, "Subgrid-scale stress modelling based on the square of the velocity gradient tensor," Flow, Turbul. Combust **62**, 183–200 (1999).
[5]J. Larsson and Q. Wang, "The prospect of using large eddy and detached eddy simulations in engineering design, and the research required to get there," Philos. Trans. R. Soc. A **372**, 20130329 (2014).
[6]C. G. Speziale, "Computing non-equilibrium turbulent flows with time-dependent RANS and VLES," in *Fifteenth International Conference on Numerical Methods in Fluid Dynamics* (Springer, 1997), pp. 123–129.
[7]P. R. Spalart, W. H. Jou, M. Strelets, and S. R. Allmaras, "Comments on the feasibility of LES for wings, and on a hybrid RANS/LES approach," in *Proceedings of the First AFOSR International Conference on DNS/LES* (Greyden Press, 1997), pp. 137–147.
[8]J. Fröhlich and D. von Terzi, "Hybrid LES/RANS methods for the simulation of turbulent flows," Prog. Aerosp. Sci. **44**, 349–377 (2008).
[9]P. Sagaut, *Large Eddy Simulation for Incompressible Flows: An Introduction* (Springer Science + Business Media, 2006).
[10]P. Sagaut, *Multiscale and Multiresolution Approaches in Turbulence: LES, DES and Hybrid RANS/LES Methods: Applications and Guidelines* (World Scientific, 2013).
[11]J. Holgate, A. Skillen, T. Craft, and A. Revell, "A review of embedded large eddy simulation for internal flows," Arch. Comput. Methods Eng. **26**, 865–882 (2019).
[12]P. R. Spalart, S. Deck, M. L. Shur, K. D. Squires, M. K. Strelets, and A. Travin, "A new version of detached-eddy simulation, resistant to ambiguous grid densities," Theor. Comput. Fluid Dyn. **20**, 181–195 (2006).
[13]M. L. Shur, P. R. Spalart, M. K. Strelets, and A. K. Travin, "A hybrid RANS-LES approach with delayed-DES and wall-modelled LES capabilities," Int. J. Heat Fluid Flow **29**, 1638–1649 (2008).
[14]H. Gopalan and R. Jaiman, "Numerical study of the flow interference between tandem cylinders employing non-linear hybrid URANS–LES methods," J. Wind Eng. Ind. Aerodyn. **142**, 111–129 (2015).
[15]P. Batten, U. Goldberg, and S. Chakravarthy, "Sub-grid turbulence modeling for unsteady flow with acoustic resonance," in *38th Aerospace Sciences Meeting and Exhibit* (AIAA, 2000), p. 473.
[16]B. Chaouat and R. Schiestel, "Partially integrated transport modeling method for turbulence simulation with variable filters," Phys. Fluids **25**, 125102 (2013).
[17]B. Chaouat and R. Schiestel, "A new partially integrated transport model for subgrid-scale stresses and dissipation rate for turbulent developing flows," Phys. Fluids **17**, 65106 (2005).
[18]J. B. Perot and J. Gadebusch, "A stress transport equation model for simulating turbulence at any mesh resolution," Theor. Comput. Fluid Dyn. **23**, 271–286 (2009).

[19]J. B. Perot and J. Gadebusch, "A self-adapting turbulence model for flow simulation at any mesh resolution," Phys. Fluids **19**, 115105 (2007).
[20]H. Xiao, J.-X. Wang, and P. Jenny, "An implicitly consistent formulation of a dual-mesh hybrid LES/RANS method," Commun. Comput. Phys. **21**, 570–599 (2017).
[21]P. T. L. Nguyen, J. C. Uribe, I. Afgan, and D. R. Laurence, "A dual-grid hybrid RANS/LES model for under-resolved near-wall regions and its application to heated and separating flows," Flow, Turbul. Combust. **104**(2019), 835–859 (2020).
[22]A. E. A. Ali, I. Afgan, D. Laurence, and A. Revell, "A dual-mesh hybrid RANS-LES simulation of the buoyant flow in a differentially heated square cavity with an improved resolution criterion," Comput. Fluids **224**, 104949 (2021).
[23]L. Davidson, "Evaluation of the SST-SAS model: Channel flow, asymmetric diffuser and axi-symmetric hill," in European Community on Computational Methods in Applied Sciences (ECCOMAS CFD) (2006).
[24]S. E. Gant, "Reliability issues of LES-related approaches in an industrial context," Flow, Turbul. Combust **84**, 325–335 (2010).
[25]M. S. Gritskevich, A. V. Garbaruk, T. Frank, and F. R. Menter, "Investigation of the thermal mixing in a T-junction flow with different SRS approaches," Nucl. Eng. Des. **279**, 83–90 (2014).
[26]P. R. Spalart, "Detached-eddy simulation," Annu. Rev. Fluid Mech. **41**, 181–202 (2009).
[27]B. L. Smith, J. H. Mahaffy, and K. Angele, "A CFD benchmarking exercise based on flow mixing in a T-junction," Nucl. Eng. Des **264**, 80–88 (2013).
[28]F. R. Menter and Y. Egorov, "A scale-adaptive simulation model using two-equation models," in *43rd AIAA Aerospace Sciences Meeting and Exhibit* (AIAA, 2005), pp. 1–13.
[29]F. Menter, M. Kuntz, and R. Bender, "A scale-adaptive simulation model for turbulent flow predictions," in *41st Aerospace Sciences Meeting and Exhibit* (AIAA, 2003), pp. 1–12.
[30]S. Girimaji, "Partially-averaged Navier-Stokes model of turbulence: A Reynolds-averaged Navier-Stokes to direct numerical simulation bridging method," J. Appl. Mech. **73**, 413–421 (2006).
[31]S. Heinz, "The large eddy simulation capability of Reynolds-averaged Navier-Stokes equations: Analytical results," Phys. Fluids **31**, 021702 (2019).
[32]S. Girimaji and K. Abdol-Hamid, "Partially-averaged Navier Stokes model for turbulence: Implementation and validation," in *43rd AIAA Aerospace Sciences Meeting and Exhibit* (AIAA, 2005), pp. 1–14.
[33]D. Basu, A. Hamed, and K. Das, "Assessment of partially averaged Navier Stokes (PANS) multiscale model in transonic turbulent separated flows," in *ASME/JSME 5th Joint Fluids Engineering Conference* (ASME, 2007), pp. 1451–1459.
[34]A. Elmiligui, K. Abdol-Hamid, S. Massey, and S. Pao, "Numerical study of flow past a circular cylinder using RANS, Hybrid RANS/LES and PANS formulations," in *22nd Applied Aerodynamics Conference and Exhibit* (AIAA, 2004).
[35]G. Lenci and E. Baglietto, "A structure-based approach for topological resolution of coherent turbulence: Overview and demonstration," in *16th International Topical Meeting on Nuclear Reactor Thermal Hydraulics* (ANS, 2015), pp. 1–14.
[36]G. Lenci, "A methodology based on local resolution of turbulent structures for effective modeling of unsteady flows," Ph.D. thesis (Massachusetts Institute of Technology, 2016), available at http://doi.org/1721.1/106701.
[37]E. Baglietto and H. Ninokata, "Anisotropic eddy viscosity modeling for application to industrial engineering internal flows," Int. J. Transp. Phenom. **8**, 109 (2006).
[38]J. Feng, T. Frahi, and E. Baglietto, "STRUCTure-based URANS simulations of thermal mixing in T-junctions," Nucl. Eng. Des. **340**, 275–299 (2018).
[39]L. Xu, "A second generation URANS approach for application to aerodynamic design and optimization in the automotive industry," Ph.D. thesis (Massachusetts Institute of Technology, 2020), available at https://doi.org/1721.1/127734.
[40]J. Feng, M. Acton, E. Baglietto, A. R. Kraus, and E. Merzari, "On the relevance of turbulent structures resolution for cross-flow in a helical-coil tube bundle," Ann. Nucl. Energy **140**, 107298 (2020).
[41]M. Acton, G. Lenci, and E. Baglietto, "Structure-based resolution of turbulence for sodium fast reactor thermal striping applications," in *16th International Topical Meeting on Nuclear Reactor Thermal Hydraulics* (ANS, 2015).
[42]C. Wang, F. Wang, C. Li, C. Ye, T. Yan, and Z. Zou, "A modified STRUCT model for efficient engineering computations of turbulent flows in hydro-energy machinery," Int. J. Heat Fluid Flow **85**, 108628 (2020).
[43]J. A. Schneider, M. H. Anderson, E. Baglietto, L. Bilbao, M. Bucknor, S. Morgan, M. Weatherhead, Z. Wu, and L. Xu, "Thermal stratification modeling and analysis for sodium fast reactor technology," in *ANS Winter Meeting* (ANS, 2018).
[44]E. Baglietto, G. Lenci, and D. Concu, "STRUCT: A second-generation urans approach for effective design of advanced systems," in Fluids Engineering Division Summer Meeting (2017), available at http://doi.org/1721.1/117004.
[45]K. Yau, "Application of hybrid CFD turbulence model, STRUCT-ε, on heated flow cases," Master thesis (Massachusetts Institute of Technology, 2019), available at https://doi.org/1721.1/123357.
[46]J. García, J. Muñoz-Paniagua, L. Xu, and E. Baglietto, "A second-generation URANS model (STRUCT-ε) applied to simplified freight trains," J. Wind Eng. Ind. Aerodyn. **205**, 104327 (2020).
[47]C. Wang, F. Wang, C. Ye, B. Wang, and Z. Zou, "Application of the MST turbulence model to predict the tip leakage vortex flows," Eng. Comput. **38**, 344–353 (2020).
[48]J. Feng, E. Baglietto, K. Tanimoto, and Y. Kondo, "Demonstration of the STRUCT turbulence model for mesh consistent resolution of unsteady thermal mixing in a T-junction," Nucl. Eng. Des. **361**, 110572 (2020).
[49]E. Baglietto and H. Ninokata, "Improved turbulence modeling for performance evaluation of novel fuel designs," Nucl. Technol. **158**, 237–248 (2007).
[50]N. S. Liu and T. H. Shih, "Turbulence modeling for very large-eddy simulation," AIAA J. **44**, 687–697 (2006).
[51]J. C. R. Hunt, A. A. Wray, and P. Moin, "Eddies, streams, and convergence zones in turbulent flows," in *Proceedings of Summer Program* (NASA, 1988).
[52]C. Meneveau, T. S. Lund, and W. H. Cabot, "A Lagrangian dynamic subgrid-scale model of turbulence," J. Fluid Mech. **319**, 353–385 (1996).
[53]M. Germano, "Fundamentals of large eddy simulation," Adv. Turbul. Flow Comput. **395**, 81–130 (2000).
[54]J. Feng and E. Baglietto, "Thermal mixing test for STRUCT benchmark," Report (Mitsubishi Heavy Industry, LTD, 2018).
[55]S. B. Pope, *Turbulent Flows* (Cambridge University Press, 2001).
[56]F. S. Lien, W. L. Chen, and M. A. Leschziner, "Low-Reynolds-number eddy-viscosity modelling based on non-linear stress-strain/vorticity relations," in *Engineering Turbulence Modelling and Measurements* (Elsevier, 1996), Vol. 3, pp. 91–100.
[57]B. E. Launder and D. B. Spalding, "The numerical computation of turbulent flows," Comput. Methods Appl. Mech. Eng. **3**, 269–289 (1974).
[58]J. Boussinesq, "Essai sur la théorie des eaux courantes," Comptes rendus de l'Académie des Sciences **23**, 1–680 (1877).
[59]E. Baglietto, H. Ninokata, and T. Misawa, "CFD and DNS methodologies development for fuel bundle simulations," Nucl. Eng. Des. **236**, 1503–1510 (2006).
[60]E. Baglietto and H. Ninokata, "A turbulence model study for simulating flow inside tight lattice rod bundles," Nucl. Eng. Des. **235**, 773–784 (2005).
[61]D. A. Lyn, S. Einav, W. Rodi, and J. H. Park, "A laser-Doppler velocimetry study of ensemble-averaged characteristics of the turbulent near wake of a square cylinder," J. Fluid Mech. **304**, 285–319 (1995).
[62]B. L. Smith, J. H. Mahaffy, K. Angele, and J. Westin, "Report of the OECD/NEA—Vattenfall T-junction Benchmark exercise," Report No. NEA/CSNI/R(2011)5 (NEA/CSNI, 2011).
[63]C. U. Buice, "Experimental investigation of flow through an asymmetric plane diffuser," Ph.D. thesis (Stanford University, 1997).
[64]S. V. Patankar and D. B. Spalding, "A calculation procedure for heat, mass and momentum transfer in three-dimensional parabolic flows," Int. J. Heat Mass Transfer **15**, 1787–1806 (1972).
[65]C. M. Rhie and W. L. Chow, "Numerical study of the turbulent flow past an airfoil with trailing edge separation," AIAA J. **21**, 1525–1532 (1983).
[66]L. W. Hu and M. S. Kazimi, "LES benchmark study of high cycle temperature fluctuations caused by thermal striping in a mixing tee," Int. J. Heat Fluid Flow **27**, 54–64 (2006).
[67]R. A. Berdanier, "Turbulent flow through an asymmetric plane diffuser," Master thesis (Purdue University, 2011), available at https://doi.org/10.13140/RG.2.1.3001.7367.